Coupled geomechanical and seismic modeling of compaction-induced traveltime shifts for multicomponent data

Steven Smith & Ilya Tsvankin
Colorado School of Mines, Center for Wave Phenomena, Golden Colorado

ABSTRACT
Time-lapse seismic methods have proven successful in evaluating changes in reservoirs caused by production. Accurate modeling of compaction-related time shifts requires combining geomechanics with full-waveform simulation of seismic data. Here, we study the influence of compaction-induced stress and strain around a reservoir on compressional (P), mode-converted (PS), and shear (S) waves. Geomechanical reservoir models are used to generate stress-related stiffness coefficients, which serve as input to 2D anisotropic finite-difference modeling. Reflectors are placed at multiple depths to evaluate time-lapse anomalies for different source locations and a wide range of reservoir pressure. The baseline and monitor shot records are processed by windowed cross-correlation analysis to compute "visualization surfaces" of time shifts with respect to the baseline survey. Our modeling results show that the spatial pattern of time shifts for PS- and S-waves is generally similar to that for P-waves. However, while P-wave traveltimes above the reservoir increase after compaction, PS- and S-wave traveltimes there are slightly reduced. The traveltimes of all modes decrease for reflectors below the stressed reservoir. Almost constant time shifts of PS- and S-waves for a range of offsets and source locations indicate that the contribution of stress-induced velocity anisotropy to shear-wave signatures is weak, because the symmetry is close to elliptical. The developed methodology not only helps understand the behavior of traveltime shifts for PS- and S-waves, but can be used in the inversion for the stress field.

Key words: geomechanics, seismic modeling, stress-induced anisotropy, converted waves, shear waves, time-lapse, compacting reservoir, transverse isotropy, VTI

Introduction

General Overview

Time-lapse (4D) monitoring of oil and gas reservoirs is based on estimating the differences between seismic signatures measured for baseline and monitor surveys (Calvert, 2005). Pore-pressure reduction inside a reservoir causes stress, strain, and impedance changes throughout the section. The type, magnitude, and spatial distribution of differences between time-lapse data sets allow production engineers and interpreters to map oil drainage patterns and reservoir block connectivity. This information is helpful in enhanced recovery operations, such as fracturing and flooding.

Production-induced stress fields depend on both volumetric and shear strains associated with changes in pore fluid pressure and bulk modulus of the reservoir. In addition to pressure drop and impedance variations within the reservoir, the surrounding rock undergoes stress and strain redistribution. Compaction-induced stress and strain in the overburden can create or reactivate normal and reverse faults, resulting in small to moderate earthquakes in close proximity to the reservoir (Zoback, 2007). Concentrated regions

of high subsurface stress (Bachrach et al., 2007) may cause shearing of wells, which must then be abandoned, repaired, or side-tracked to resume production. An example of widespread stress/compaction damage is found in Wilmington Field, Long Beach, California. This field experienced approximately 30 feet of subsidence from 1931-1952, with significant damage to over 200 production wells, associated infrastructure, bridges, and wharfs of the Terminal Island area in Long Beach (McCann and Wilts, 1951; Strehle, 1987).

Time-lapse seismic data are often migrated to generate images reflecting changes in the reservoir. Signatures measured in time-lapse surveys also have potential for estimating subsurface stress. Synthetic modeling of pore-pressure-dependent time shifts for multiple horizons above and below the reservoir can be used to study the influence of spatially varying stresses on the kinematics of reflected waves. Traveltime shifts, coupled with well-pressure histories, can serve as input to inversion algorithms designed to reconstruct reservoir pressure at locations distant from existing wells. Time-shift measurements for reflectors and events most sensitive to changes in reservoir pressure and stress may be exploited to devise a flexible monitoring program that reduces repetition of full-scale monitoring surveys.

In this paper, we describe a method for semi-coupled geomechanical and full-waveform seismic modeling of multicomponent data acquired above compacting reservoirs. First, we review recent advances in the field of uniaxial/vertical stress compaction and time-lapse processes in the reservoir. We also discuss the work of Fuck et al. (2009, 2010), who studied the influence of compaction-induced stress and strain on the velocity field and P-wave time shifts using the nonlinear theory of elasticity. Then we introduce our semi-coupled geomechanical/seismic modeling methodology and describe the time shifts of P-, PS-, and S-waves for a simple model of a rectangular reservoir embedded in a homogeneous host rock.

Compaction-Induced Velocity Perturbations

Compaction and Stress

A number of recent publications discuss seismic time shifts associated with compaction, subsidence and related subsurface stress perturbations. These approaches typically involve some form of "semi-coupled" geomechanical and seismic modeling. Semi-coupled models cyclically solve systems of equations for interrelated processes, but the partial differential equations (PDEs) and their solvers remain separate; for example, wave-propagation PDEs are not directly coupled to Navier stress/strain PDEs (Olden et al., 2001; Minkoff et al., 2004; Sen and Settari, 2005). Most existing studies have been limited to evaluation of vertical stress/strain and analysis of time shifts on stacked/zero-offset data (Hatchell and Bourne, 2005; Roste, 2007; Landrø and Stammeijer, 2004). Zero-offset time shifts can help estimate the change in the reservoir thickness, allowing improved monitoring of reservoir volume (i.e., barrels-in-place). Traveltime perturbations obtained from uniaxial compaction models are particularly significant for soft reservoir rock. However, more general stress-based formulations (including triaxial stress) help constrain the deviatoric stress tensor responsible for stress-induced anisotropy (Fuck et al., 2009). Heterogeneous, anisotropic velocity fields caused by reservoir compaction result in perturbations of shear-wave splitting and azimuthally varying moveout velocity (Olofsson et al., 2003; Herwanger and Horne, 2009).

P-wave Time Shifts

It has been shown that reservoir compaction induces stress changes resulting in spatially varying, anisotropic velocity fields inside and outside the reservoir (Herwanger and Horne, 2005; Herwanger et al., 2007; Fuck et al., 2009). For 2D reservoir models, the stress-induced symmetry is transversely isotropic, with a nearly vertical symmetry axis (VTI); the symmetry axis noticeably deviates from the vertical only near the reservoir corners (Fuck et al., 2009). Fuck and Tsvankin (2009), Prioul et al. (2004), and Shapiro and Kaselow (2005) show that stress-induced anisotropy is close to elliptical, with approximately equal values of the anisotropy parameters ϵ and δ.

Fuck et al. (2009) analyze stress-induced anisotropy caused by a pore pressure drop in a rectangular reservoir embedded in originally homogeneous host rock (Figure 1). They derive an approximate expression for traveltime changes by using the nonlinear theory of elasticity and evaluating traveltime perturbations along reference rays traced through an unstressed background. Fuck et al. (2009) also model compaction-induced P-wave time shifts using anisotropic ray tracing for the reservoir model in Figure 1. They demonstrate that traveltime shifts are controlled by the combination of volumetric and deviatoric strains. The volumetric strain, given by

$$\Delta e_{kk} = \frac{1}{3}\left(\Delta\epsilon_{11} + \Delta\epsilon_{22} + \Delta\epsilon_{33}\right). \qquad (1)$$

is significant only inside the reservoir ($\Delta\epsilon_{ii}$ is the dilatation component along the ith axis). Therefore, traveltime shifts for reflections above the reservoir are generated by deviatoric stress and strains. The most significant time shifts, however, occur for reflectors beneath the reservoir. Raypaths for these events are influenced by the deviatoric stress around of the reservoir, but also pass through the reservoir itself, which experiences the bulk of compaction-induced volumetric strain (Δe_{kk}). Fuck et al. (2009) demonstrate that offset variations of time shifts for reflections both above and below the reservoir are largely controlled by the deviatoric strains responsible for velocity anisotropy. Figure

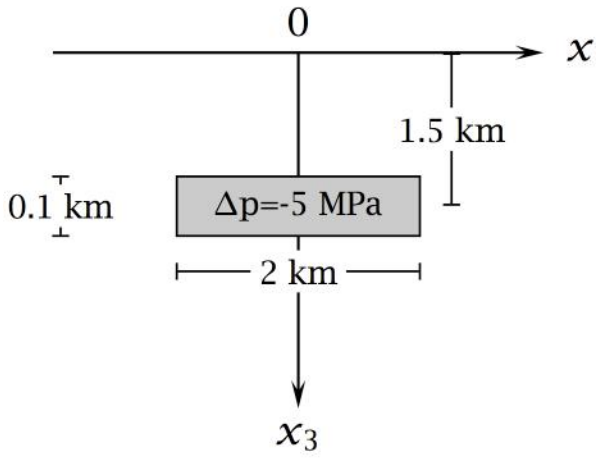

Figure 1. Reservoir geometry used by Fuck (2009) and Fuck et al. (2009). Pore-pressure ($P_{\rm p}$) reduction occurs only within the reservoir, resulting in an anisotropic velocity field due to the excess stress and strain. For geomechanical modeling, the reservoir is located in a model-space measuring $20,000 \times 10,000$ m. The model dimensions are sufficient for obtaining stress, strain, and displacement which are close to those for an infinite medium. The reservoir is comprised of and embedded in homogeneous Berea sandstone (ρ = 2140 kg/m^3, V$_P$ = 2300 m/s, V_S = 1456 m/s) with the following, density-normalized third-order stiffness coefficients: $C_{111}/\rho = -13,904$ GPa, $C_{112}/\rho = 533$ GPa, and $C_{155}/\rho = 481$ GPa (Prioul et al., 2004). The Biot coefficient is set to 0.85. Velocities in the model are reduced by 10% from the laboratory values to account for the difference between static and dynamic stiffnesses in low-porosity rocks (Yale and Jamieson, 1994). Here, we analyze PS- and S-wave time shifts for this model for 5 MPa and 20 MPa pore-pressure drops.

2 shows both the magnitude and spatial distribution of P-wave traveltime perturbations obtained by ray tracing around the rectangular reservoir in Figure 1. If the unstressed medium is not homogeneous, the contrast in the rigidity modulus μ between the reservoir and surrounding rock influences the stress/strain perturbation inside and near the reservoir (Fuck et al., 2010).

Seismic velocities change when the local stiffnesses of the rock are altered due to compression or shearing. This change for linearly elastic materials can be described using Hooke's law:

$$s_{ij} = c_{ijkl}\,\epsilon_{kl}, \tag{2}$$

where $\mathbf{s}$ is the stress tensor (denoted by $\mathbf{s}$ to avoid confusion with the anisotropy parameter σ), and ϵ is the strain tensor. Equation 2 implicitly assumes that the stiffness coefficients relating stress to strain remain constant. The stiffnesses, however, change as a function of strain (Prioul et al., 2004; Fuck et al., 2009):

$$c_{ijkl} = c^{o}_{ijkl} + \frac{\partial c_{ijkl}}{\epsilon_{mn}}\,\Delta\epsilon_{mn} = c^{o}_{ijkl} + c_{ijklmn}\,\Delta\epsilon_{mn}. \tag{3}$$

In the Voigt matrix notation, equation 3 can be written as

$$C_{\alpha\beta} = C^{o}_{\alpha\beta} + C_{\alpha\beta\gamma}\,\Delta\epsilon_{\gamma}. \tag{4}$$

The third-order stiffness coefficients c_{ijklmn} are derived from higher-order terms of the strain-energy function (Hearmon, 1953; Sarkar et al., 2003; Prioul et al., 2004). The strain-induced changes in stiffness described by equations 3 and 4 result in spatially varying stiffness/velocity perturbations around a compacting reservoir. The Voigt matrix notation is convenient because it simplifies the summation in equation 3 and analysis of the symmetry of the strain-induced velocity field (Fuck and Tsvankin, 2009).

Fuck et al. (2009) express the P-wave traveltime in a stressed medium as the sum of the isotropic background traveltime and a perturbation that depends on the stress-induced stiffness changes. Application of equations 3 and 4 yields compaction-related time shifts as a function of two independent third-order coefficients – C_{111} and C_{112}.

Experimentally obtained $C_{\alpha\beta}$ values (Prioul et al., 2004) make it possible to model changes in the stiffness coefficients caused by stress/strain applied to an isotropic medium. Triaxial compaction-related stress causes a combination of volumetric and deviatoric strain perturbations resulting in orthorhombic symmetry. In two dimensions the symmetry is transversely isotropic, as discussed above.

The spatial distribution of the compaction-induced stress/strain may be complex, depending on the background properties and the structural geology/petrology of the reservoir (Fuck, 2009; Fuck et al., 2010). Additional complexity is caused by pronounced reservoir heterogeneity An example would be a tilted reservoir with multiple aggregate bulk moduli caused by the natural separation of brine and liquid/gas hydrocarbons (Johnston, 2010).

Methodology

We devised a modeling methodology and software package to study time-lapse multicomponent wavefields for compacting reservoirs. 2D, semi-coupled geomechanical and full-waveform modeling was implemented employing an approach similar to that of Minkoff et al. (2004), Herwanger and Horne (2005), Herwanger and Horne (2009) and Fuck (2009). The methodology can handle multi-compartment reservoirs of various shapes, depths, tilts, and independent pressure histories.

Compaction-induced displacement, strain, and stresses for our geomechanical reservoir models are computed using COMSOL PDE software (COMSOL AB, 2008). Geomechanical physics for a subsurface inclusion such as a reservoir are described by Zoback (2007). The fluid within the reservoir is under pore pressure ($P_{\rm p}$) that counteracts overburden stress. Another pressure

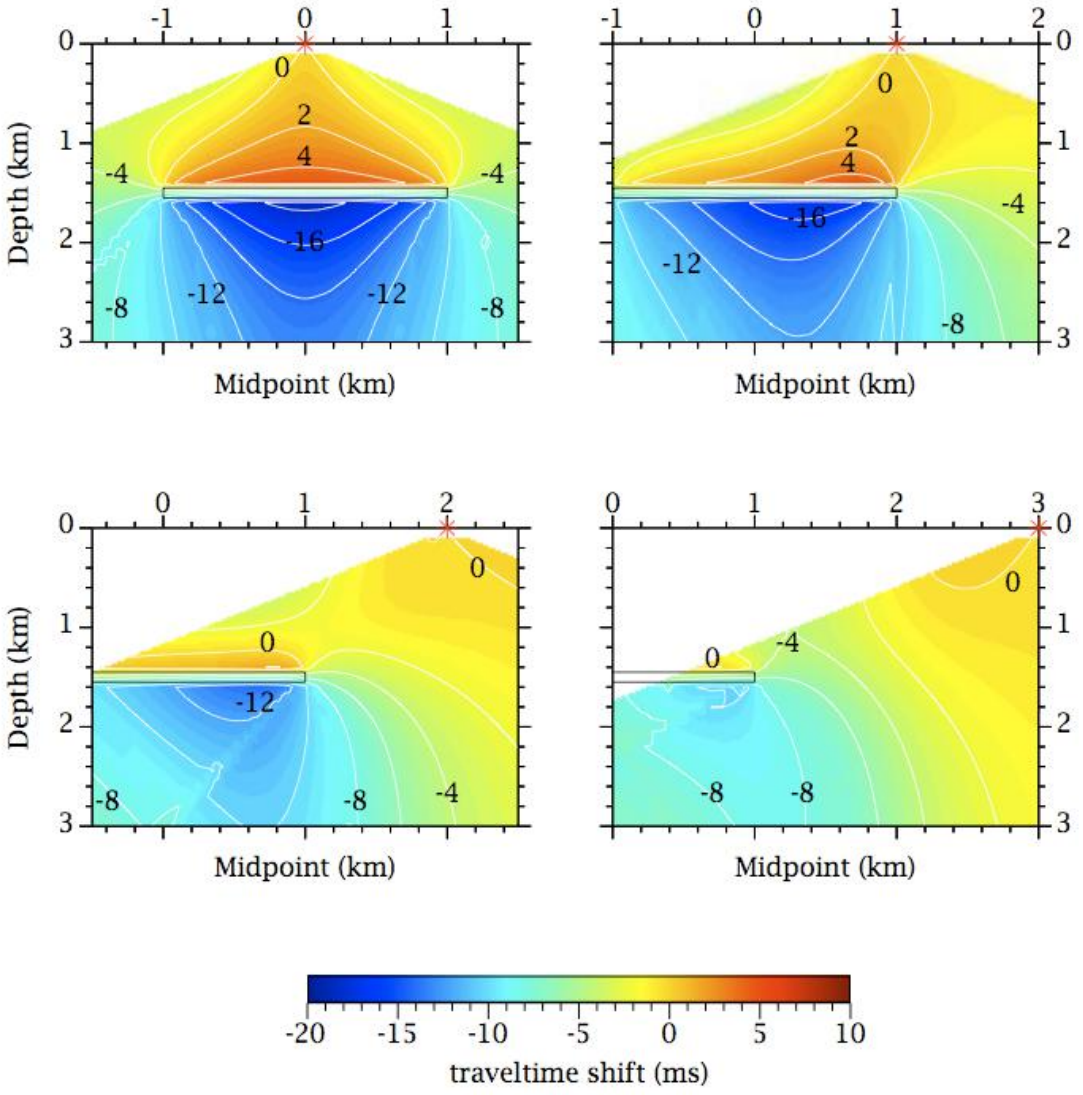

Figure 2. P-wave traveltime shifts computed by ray tracing for the model from Figure 1 (after Fuck et al. (2009)). The asterisk marks the source location at the surface. The time shift (ms) shown at each (X,Z) point corresponds to the reflection form a horizontal interface at depth Z recorded at the source-receiver offset $2\,(X - X_0)$, where X_0 is the source coordinate.

component is provided by grain-to-grain contact in the matrix via the viscoelastic Biot coefficient α:

$$P_{\rm bulk} \simeq P_{\rm p} + P_{\rm matrix} \simeq \alpha P, \tag{5}$$

with

$$\alpha = 1 - \frac{K_{\rm a}}{K_{\rm g}}, \tag{6}$$

where $K_{\rm a}$ is the aggregate bulk modulus of the rock frame and fluids, and $K_{\rm g}$ is the bulk modulus of the grain material (Mavko et al., 2003). Initially, the system is assumed to be in hydrostatic equilibrium such that the reservoir pressure balances that of the overburden column:

$$P_{\rm res} = P_{\rm over}, \tag{7}$$

$$\alpha P_{\rm p} = \left(1 - \frac{K_{\rm a}}{K_{\rm g}}\right) P_{\rm p} = \rho_{\rm over} * g * z_{\rm res}. \tag{8}$$

Changes in reservoir pressure are due just to changes in the pore fluid pressure $P_{\rm p}$. These pressure changes are linear, and are used as the force function for the Navier equation $[-\nabla \cdot (c\nabla \mathbf{u}) = \mathbf{F}]$ governing the system's stress state (COMSOL AB, 2008). Due to the presence of the Biot coefficient, the pore pressure needed

to maintain equilibrium results in an overpressured reservoir volume, which is typical for a freshly tapped reservoir. As verified by Fuck et al. (2009), the resulting numerical stress/strain fields for a rectangular inclusion are close to analytic solutions obtained by Hu (1989).

The resulting stress/strain fields are processed with an algorithm based on the nonlinear theory of elasticity to calculate the stiffness coefficients (Fuck et al., 2009). These stiffnesses serve as input to the SFEWE 2D anisotropic finite-difference modeling code (Sava and Godwin, 2010), which generates multicomponent seismic data. The SFEWE software excites both P- and S-waves by applying directional forces oriented along the X and Z axes. The source signal is a Ricker wavelet with a center frequency of 44 Hz and an effective bandwidth of approximately 110 Hz. Time shifts for P, PSV, and SV waves are measured from the modeled wavefields by computing cross-correlations of windowed arrivals in the baseline and monitor surveys; the windowing is performed along the best-fit moveout curves.

Synthetic Test

We test our software package on the reservoir model of Fuck et al. (2009) in Figure 1. Use of homogeneous material in the geomechanical modeling is justified for two reasons. First, Kosloff et al. (1980a) advocate the use of homogeneous media at basin scales because depositional formations outside the reservoir are typically composed of uniform source sediments. Second, we aim to observe only the influence of stress-induced anisotropy in the reservoir and overburden. Further, Fuck et al. (2010) show that the impact of background heterogeneity around the reservoir is generally insignificant. Reservoir geometry simulates a simplest case scenario, such as a fault-bound, relay-ramp block trap in a rift system like the North Sea, similar to Heidrun field (Whitley, 1992). The pore pressure reductions of 5 MPa and 20 MPa typically correspond to small to moderate reservoir pressure changes (Zoback, 2007). The use of anisotropic finite-different seismic modeling is important because it generates both kinematic and amplitude information. Furthermore, the output of the modeling code requires processing techniques that could be used on actual field data.

To evaluate depth-dependent time shifts for the reservoir located at 1500 m, a 10-m thin reflecting layer is moved downward through the model. This reflector has a high density of 3000 kg/m^3 in order to generate sufficiently large reflection amplitudes. The reflector is so thin that it is not expected to perturb the overall structure of the heterogeneous stress, strain, and stiffness changes. Baseline and monitor wavefields are computed separately for each reflector to eliminate interference with multiple reflections. For the 2D (X-Z plane) geometry used in the experiment, changes occur only in the stiffness coefficients $C_{11}, C_{13}, C_{33}, C_{55}, C_{15}$, and C_{35}, resulting in a tilted transversely isotropic (TTI) medium with a small tilt of the symmetry axis (as discussed above).

Throughout the process, the reservoir is assumed to have sufficiently large dimensions in the out-of-plane direction to allow the use of 2D modeling. We also assume that host rock with nonlinear compaction behavior may be modeled using Hooke's law with a strain-dependent set of stiffness coefficients. Compaction-induced density changes in the overburden are neglected because our software is unable to model density or porosity changes at this time.

Typical time-lapse common-shot gathers for a receiver array spanning -3000 to +3000 meters are shown in Figure 3. Here, the 10 m thin reflector is located 50 m above the top of the reservoir. The gather for the unstressed medium includes only the P-, PS-, and S-wave events from the reflector. The impedance change due to the pressure drop in the reservoir (Figure 3(b)) generates reflections from the reservoir boundaries with amplitudes comparable to those of the reflection events in Figure 3(a).

Our resulting stresses, strains, displacements, and P-wave time shifts are close to those of Fuck et al. (2009). The time shifts for the reflections from the top of the reservoir (Figure 4(a)) are close to those obtained by Fuck (2009) with ray tracing (Figure 2). Directly at the top of the reservoir the P-wave time shifts are on the order of 7-8 ms. Secondary geomechanical validation is provided by comparing our stress/strain fields to those constructed by Kosloff et al. (1980a) for the Wilmington field, with both generating surface subsidence of similar magnitude.

Analysis of Results

Our primary goal is to study the time shifts of PS- and S-waves. The SV-wave velocity in TI media (in our case, anisotropy is induced by stress) is primarily controlled by the parameter σ (Tsvankin, 2005):

$$\sigma = \left(\frac{V_{P0}}{V_{S0}}\right)^2 (\epsilon - \delta), \tag{9}$$

where V_{P0} and V_{S0} are the vertical P- and S-wave velocities. The linearized SV-wave velocity as a function of the phase angle with the symmetry axis (θ) can be written as

$$V_{SV}(\theta) = V_{S0}\left(1 + \sigma \sin^2\theta \ \cos^2\theta\right). \tag{10}$$

For elliptical anisotropy ($\epsilon = \delta$) $\sigma = 0$, $V_{SV} \approx V_{S0}$, and the velocity is independent of angle (isotropic). For example, at the center of the reservoir, computed values of σ are -0.08 for the 5 MPa pressure drop, and -0.15 for the 20 MPa pressure drop. Therefore, compaction-induced changes in the shear-wave vertical velocity have the greatest impact on PS- and S- wave time shifts

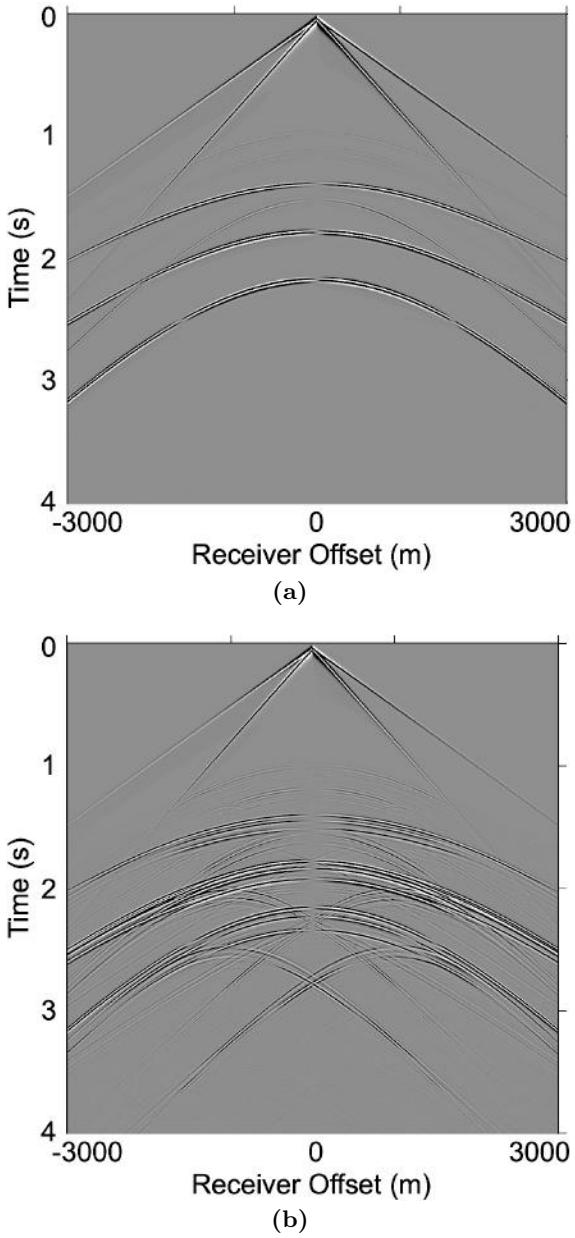

Figure 3. Common-shot gathers of the horizontal displacement for an isotropic, unstressed reservoir model (a) and for the model with the pressure drop $\Delta P_{\rm p} = 20$ MPa inside the reservoir (b) (see Figure 1). For both cases a thin, high-density reflector is positioned immediately above the reservoir at 1400 m depth (the reservoir is between 1450 m and 1550 m). The isotropic case shows clear P-, PS-, and S-wave reflections. In addition to stress-induced anisotropy, pore-pressure decrease in the reservoir alters its impedance, generating reflections and diffraction tails.

near and beneath the reservoir. Compaction-induced increases to V_{S0} inside the reservoir are approximately 270 m/s for the 5 MPa pressure drop, and 500 m/s for the 20 MPa pressure drop.

Figures 4, 5, and 6 show time shifts due to pressure drops of 5 MPa (left column) and 20 MPa (right column). Each surface is comprised of "hull curves" of time shifts computed by cross-correlation of arrivals from the set of thin reflectors placed in the stressed and unstressed models. These hull curves span the entire model from left to right at 14 depths between 200 and

3000 meters, with two reflectors positioned close to the upper and lower reservoir boundaries.

Complete time-shift plots, generated by interpolating between the hull curves, show lead/lag behavior similar to that obtained by Fuck (2009) using ray tracing (Figure 2). For all types of arrivals, time shifts above the reservoir are relatively small, with PS- and S-waves showing a traveltime decrease (or time lead), due to an increase in V_{S0} inside the reservoir. For P-waves the shifts are positive, indicating a time lag. At the top of the reservoir, Figure 4(a) shows a 5 ms P-wave lag, which is close to the 4 ms lag computed by Fuck et al. (2009) (see Figure 2 for the source coordinate $X_0 = 0$).

For all wave modes, the traveltimes for reflectors beneath the reservoir decrease after compaction because of increased velocity within the reservoir and near its edges. Time "leads" from beneath the reservoir for PS- and S-waves are approximately 2-3 times those for P-waves. When $\Delta P_{\rm p} = 20$ MPa, the time shifts of PS- and S-waves are up to two times larger than those for a drop of 5 MPa.

The reservoir and small regions at its edges experience the largest velocity changes that confine the most significant time shifts of PS- and S-waves to reflections from interfaces beneath the reservoir. The zone of largest time shifts moves laterally to the opposite side of the reservoir from the source location with increasing X-coordinate of the source. The maximum time shifts below the reservoir occur along a line connecting the source with the far edge of the reservoir because waves propagating in that direction spend the longest time in the region of the most pronounced velocity change. The small variation of S-wave time shifts with offset confirms that compaction-induced anisotropy is close to elliptical and, therefore, has weak influence on shear waves (equation 10). Time shifts for pure S-waves are controlled by the compaction-induced velocity V_{S0}. However, PS-wave offset time-shifts are slightly higher, indicating that their P-wave branch experiences increased time shifts with offset due to the stress-induced anisotropy.

Limitations

Although the general behavior of the delay surfaces correctly describes expected time shifts, there are anomalies indicative of processing artifacts. For example, an unusually large time-lead occurs on the SV data at approximately 1000-1400 m depth, and $\pm$1800 m offset. Similarly implausible time shifts are observed at a depth close to 2000-2500 m and extreme left-hand offsets of the PS data. These anomalies are caused by diffraction tails from the edges of the reservoir interfering with returns from the thin reflector (for example, see Figure 3(b)). This issue becomes more serious when the impedance contrast between the reservoir and host rock increases for larger pressure drops $\Delta P_{\rm p}$. We fit the cross-correlation timeshift curves with a user-adjustable low-pass filter and produce smoothed time-delay measurements that follow the general trend of actual time shifts. However, the combination of diffraction-tail interference or cross-correlation jitter with the current smoothing filter can cause noticeable anomalies. Post-processing improvements can overcome this issue. Despite the limited number of anomalies related to cross-correlation difficulties, the modeling package reveals correct general trends in the data.

Conclusions

Using semi-coupled geomechanical and finite-difference seismic modeling, we have developed a methodology for simulating the influence of reservoir compaction on P-, PS-, and S-wave reflections. Our process combines geomechanical computation of stresses, strains and strain-induced stiffnesses perturbations with 2D full-waveform (finite-difference) modeling for heterogeneous, anisotropic media. Velocity perturbations generated by compaction-related stress and strain are sampled by a thin reflector moved at regular depth intervals through the model. Measurements of time shifts between stressed and unstressed reservoir models are computed using windowed cross-correlations of the baseline and monitor surveys.

Numerical results for a homogeneous model with a rectangular reservoir showed that time shifts of PS- and S-waves above the reservoir are smaller in magnitude and opposite in sign from P-wave shifts. For reflectors below reservoir, however, the PS- and S-wave time shifts are approximately two to three times the P-wave time shifts. A four-fold increase in the pressure drop from 5 MPa to 20 MPa makes the time shifts up to two times larger. Time shifts for both PS- and S-waves have a similar spatial distribution as for P-waves but with a less significant dependence on the distance of the source from the center of the reservoir ($X_0 = 0$ m). The offset variation of S-wave time shifts is weak because stress-induced anisotropy is close to elliptical, and the SV-wave velocity is almost independent of angle.

Our processing generates full-waveform, multicomponent time-lapse seismic data and time shifts that can potentially be used to invert for the subsurface stress field. Finite-difference modeling also helps compute accurate amplitudes suitable for evaluating the AVO (amplitude variation with offset) response. The software is capable of handling tilted and multi-compartment reservoirs embedded in a heterogeneous background.

Future work will include stress-dependent rock modeling using the method of Shapiro (2003) and derivation of analytic equations for describing time shifts of PS- and S-waves. Sensitivity kernel analysis of the overburden after Liu and Tromp (2006) will be employed to identify stress-sensitive acquisition geometries and wave modes suitable for "reduced-footprint" seismic

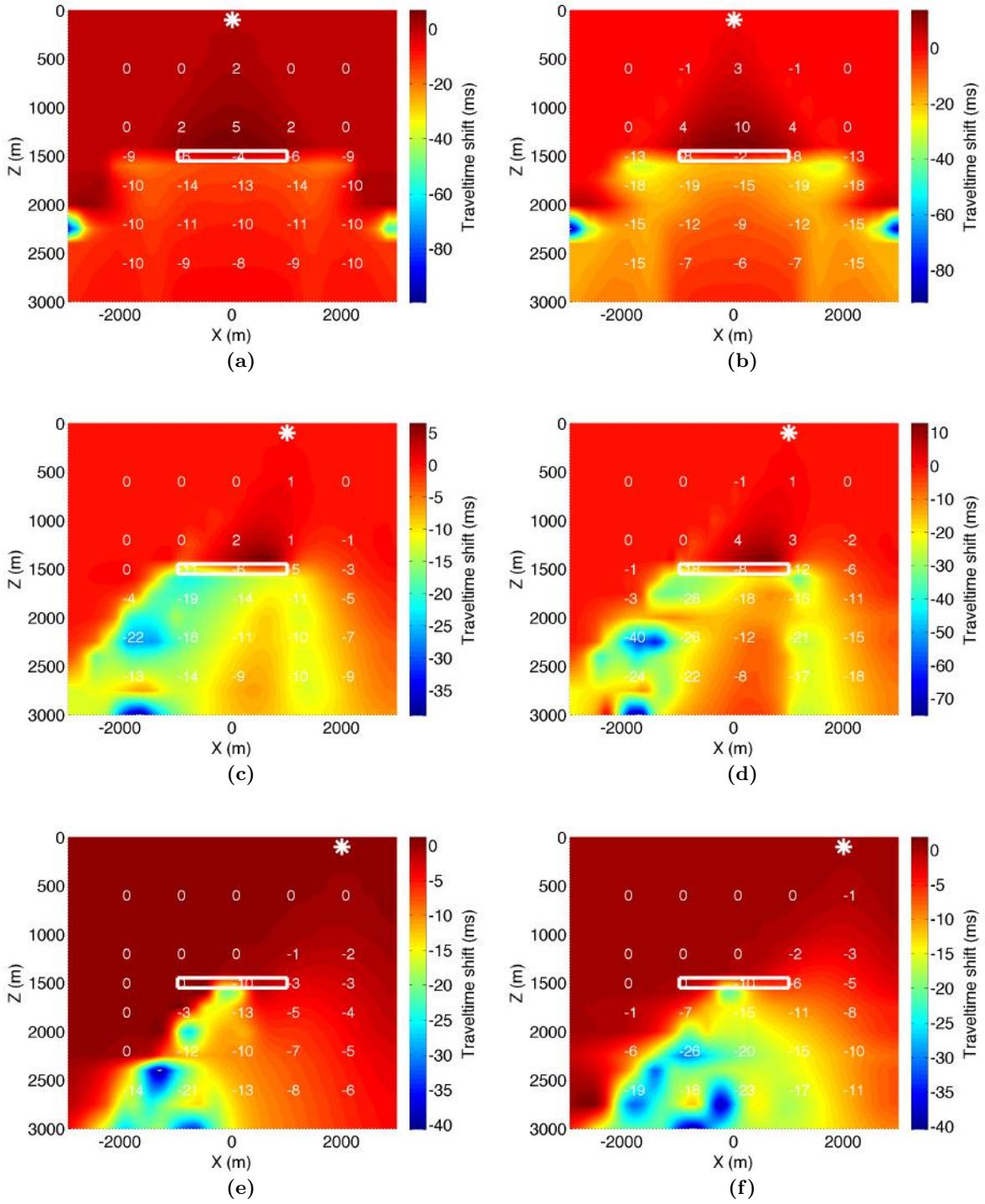

Figure 4. P-wave time shifts for the model in Figure 1 (same display as in Figure 2) produced by our modeling package for shot locations of X=0 m (a and b), X=1000 m (c and d), and X=2000 m (e and f). Pore-pressure drops are 5 MPa for the left column, and 20 MPa for the right column. The white rectangle marks the reservoir, while the white asterisk marks the shot location.

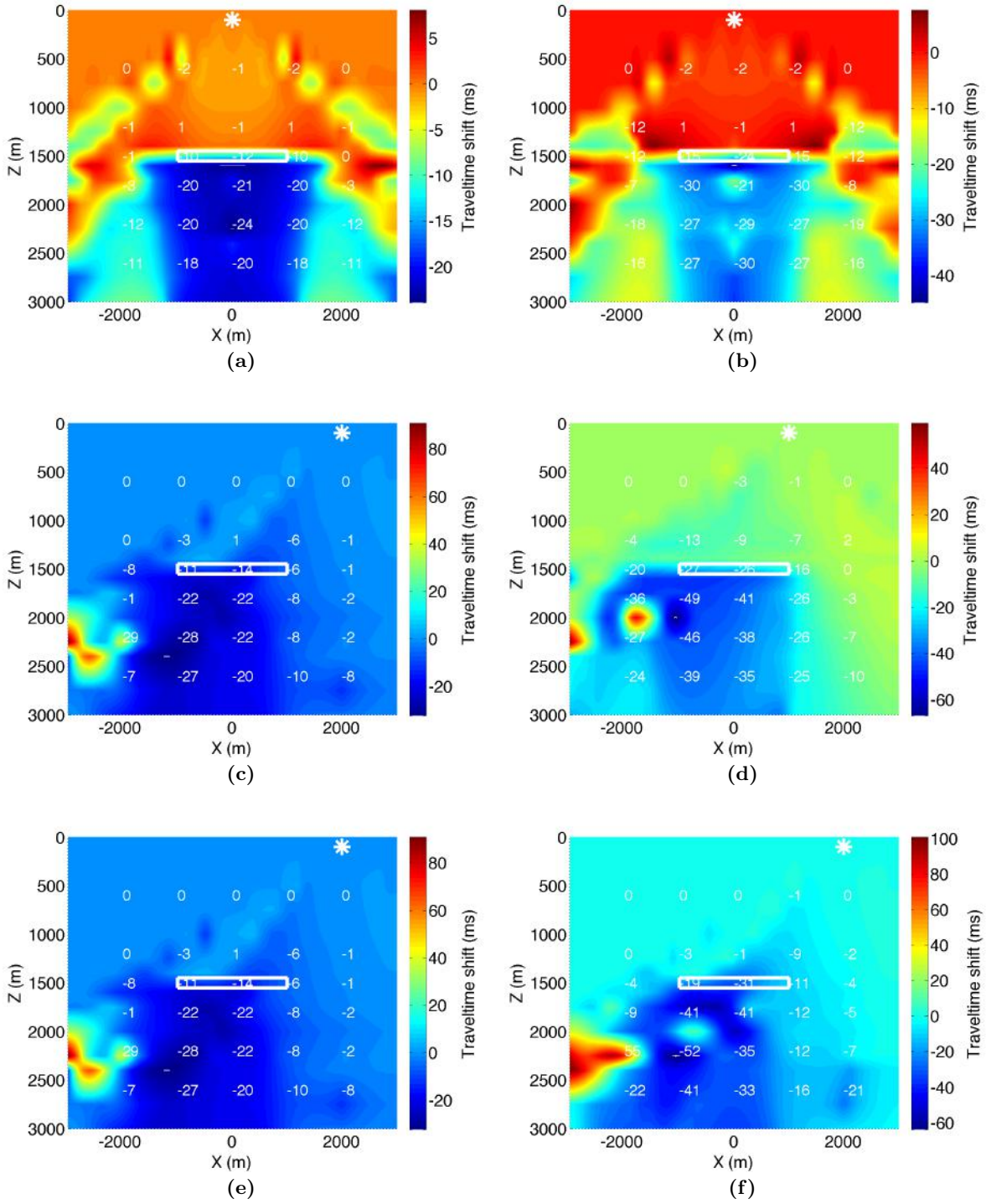

Figure 5. PS-wave time shifts for the model in Figure 1 (same display as in Figure 4) produced by our modeling package for shot locations of X=0 m (a and b), X=1000 m (c and d), and X=2000 m (e and f). Pore-pressure drops are 5 MPa for the left column, and 20 MPa for the right column.

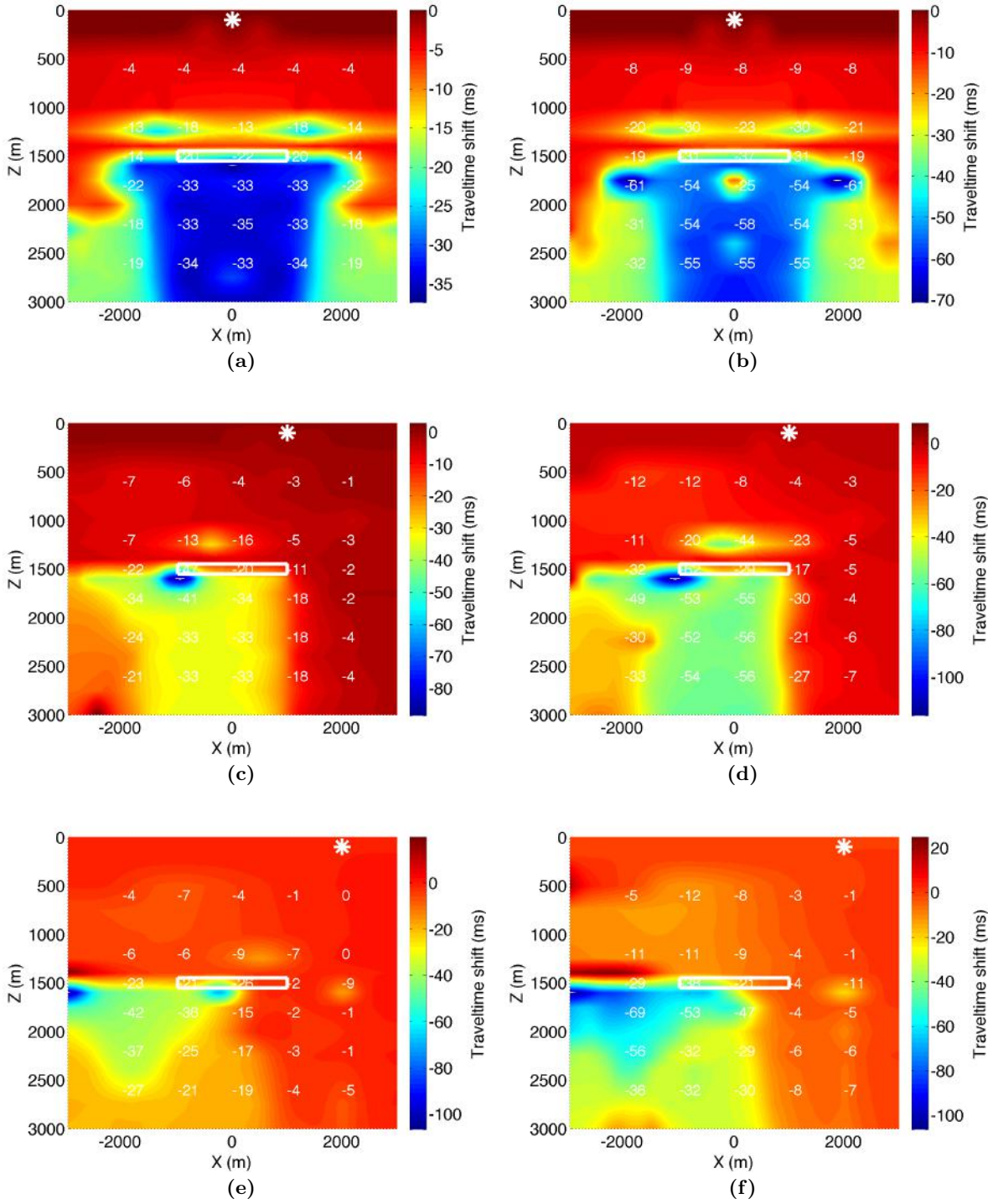

Figure 6. S-wave time shifts for the model in Figure 1 (same display as in Figure 4) produced by our modeling package for shot locations of X=0 m (a and b), X=1000 m (c and d), and X=2000 m (e and f). Pore-pressure drops are 5 MPa for the left column, and 20 MPa for the right column.

reservoir monitoring. These developments should aid in drilling and asset management for producing fields.

Acknowledgments

We wish to thank R. Fuck (Schlumberger, Cambridge), M. Batzle (CSM/CRA), A. Bakulin and J. Herwanger (WesternGeco, Houston), D. Gajewski (U. Hamburg), D. Johnston (ExxonMobil), and I. Vasconcelos (IonGeo) for discussions, comments, and suggestions, J. Godwin, T. Cullison, J. Yan (CSM/CWP), and G. M. Silva (MIT, EAPS) for assistance with Madagascar/Scons, and John Stockwell (CSM/CWP) for technical help. This work was supported by the Consortium Project on Seismic Methods for Complex Structures at CWP.

References

Bachrach, R., S. Noeth, N. Banik, M. Sengupta, G. Bunge, B. Flack, R. Utech, C. Sayers, P. Hooyman, L. de Boer, L. Leu, B. Troyer, and J. Moore, 2007, From pore-pressure prediction to reservoir characterization: A combined geomechanics-seismic inversion workflow using trend-kriging techniques in a deepwater basin: The Leading Edge, **26**, 590.

Calvert, R., 2005, Insights and methods for 4D reservoir monitoring and characterization. Distinguished Instructor Short Course, No. 8: Society of Exploration Geophysicists.

COMSOL AB, 2008, COMSOL Multiphysics. COMSOL AB, http://www.comsol.com/.

Fuck, R. F., 2009, Modeling of seismic signatures for reservoir characterization: Applications involving fracture- and stress-induced seismic velocity anisotropy: PhD thesis, Colorado School of Mines.

Fuck, R. F., A. Bakulin, and I. Tsvankin, 2009, Theory of traveltime shifts around compacting reservoirs: 3D solutions for heterogeneous anisotropic media: Geophysics, **74**, no. 1, D25–D36.

Fuck, R. F. and I. Tsvankin, 2009, Analysis of the symmetry of a stressed medium using nonlinear elasticity: Geophysics, **74**, no. 5, WB79–WB87.

Fuck, R. F., I. Tsvankin, and A. Bakulin, 2010, Influence of background heterogeneity on traveltime shifts for compacting reservoirs: submitted to Geophysics.

Hatchell, P. and S. Bourne, 2005, Rocks under strain: Strain-induced time-lapse time shifts are observed for depleting reservoirs: The Leading Edge, **24**, 1222–1225.

Hearmon, R., 1953, 'Third-Order' elastic coefficients: Acta Crystalographia, **6**, 331–340.

Herwanger, J. and S. Horne, 2005, Linking geomechanics and seismics: Stress effects on time-lapse multicomponent seismic data: 67^{th} Annual International Meeting, EAGE, Expanded Abstracts.

Herwanger, J., E. Palmer, and C. R. Schiøtt, 2007, Anisotropic velocity changes in seismic time-lapse data: 77^{th} International Meeting, SEG,Expanded Abstracts, **26**, 2883–2887.

Herwanger, J. V. and S. A. Horne, 2009, Linking reservoir geomechanics and time-lapse seismics: Predicting anisotropic velocity changes and seismic attributes: Geophysics, **74**, no. 4, W13–W33.

Hu, S. M., 1989, Stress from a parallelepipedic thermal inclusion in a semispace: Journal of Applied Physics, **66**, 2741–2743.

Johnston, D., 2010, Personal communication. ExxonMobil.

Kosloff, D., R. F. Scott, and J. Scranton, 1980a, Finite element simulation of Wilmington oil field subsidence : I. linear modelling: Tectonophysics, **65**, 339–368.

———, 1980b, Finite element simulation of Wilmington oil field subsidence: II. nonlinear modelling: Tectonophysics, **70**, 159–183.

Landrø, M. and J. Stammeijer, 2004, Quantitative estimation of compaction and velocity changes using 4D impedance and traveltime changes: Geophysics, **69**, 949.

Liu, Q. and J. Tromp, 2006, Finite-frequency kernels based on adjoint methods: Bulletin of the Seismological Society of America, **96**, 2383–2397.

Mavko, G., T. Mukerji, and J. Dvorkin, 2003, The rock physics handbook: Tools for seismic analysis in porous media: Cambridge University Press.

McCann, G. D. and C. H. Wilts, 1951, A mathematical analysis of the subsidence in the Long Beach-San Pedro area: Technical report, Caltech.

Minkoff, S. E., C. M. Stone, S. Bryant, and M. Peszynska, 2004, Coupled geomechanics and flow simulation for time-lapse seismic modeling: Geophysics, **69**, 200–211.

Olden, P., P. Corbett, R. Westerman, J. Somerville, B. Smart, and N. Koutsabeloulis, 2001, Modeling combined fluid and stress change effects in the seismic response of a producing hydrocarbon reservoir: The Leading Edge.

Olofsson, B., T. Probert, J. H. Kommedal, and O. I. Barkved, 2003, Azimuthal anisotropy from the valhall 4C 3D survey: The Leading Edge, **22**, 1228.

Prioul, R., A. Bakulin, and V. Bakulin, 2004, Nonlinear rock physics model for estimation of 3D subsurface stress in anisotropic formations: Theory and laboratory verification: Geophysics, **69**, 415.

Roste, T., 2007, Monitoring overburden and reservoir changes from prestack time-lapse seismic data - applicaitons to chalk fields: PhD thesis, Norwegian University of Science and Technology.

Sarkar, D., A. Bakulin, and R. L. Kranz, 2003, Anisotropic inversion of seismic data for stressed media: Theory and a physical modeling study on berea sandstone: Geophysics, **68**, 690.

Sava, P. and J. Godwin, 2010, SFEWE elastic fi-

nite difference wave-propagation development code for the Madagascar seismic software collection. http://www.reproducability.org.

Sen, V. and A. T. Settari, 2005, Coupled geomechanical and flow modeling of compacting reservoirs: The Leading Edge, **24**, 1284–1286.

Shapiro, S. A., 2003, Elastic piezosensitivity of porous and fractured rocks: Geophysics, **68**, 482–486.

Shapiro, S. A. and A. Kaselow, 2005, Porosity and elastic anisotropy of rocks under tectonic stress and pore-pressure changes: Geophysics, **70**, no. 5, N27–N38.

Strehle, R., 1987, Subsidence in long beach: Presented at the AAPG Pacific Section - Oil Producing Areas in Long Beach.

Tsvankin, I., 2005, Seismic signatures and analysis of reflection data in anisotropic media, volume 29. Handbook of Geophysical Exploration, Seismic Exploration: Elsevier Science.

Whitley, P. K., 1992, The geology of heidrun: A giant oil and gas field on the mid-norwegian shelf, chapter 24, 383–406. A. A. P. G, giant oil and gas fields of the decade 1978-1988 ed.

Yale and Jamieson, 1994, Static and dynamic mechanical properties of carbonates: Proceedings of the 1st Proceedings of the 1st North American Rock Mechanics Symposium, 463–471.

Zoback, M. D., 2007, Reservoir geomechanics: Cambridge University Press.